Published in final edited form as:

Cell Rep. 2022 January 18; 38(3): 110257. doi:10.1016/j.celrep.2021.110257.

Parallel processing of sensory cue and spatial information in the dentate gyrus

Sebnem N. Tuncdemir[1,2], **Andres D. Grosmark**[3], **Gergely F. Turi**[1,2], **Amei Shank**[4], **John C. Bowler**[3], **Gokhan Ordek**[2], **Attila Losonczy**[3], **Rene Hen**[1,2,5,*], **Clay O. Lacefield**[1,2,*]

[1]Department of Psychiatry, Columbia University, New York, NY 10032, USA

[2]Division of Systems Neuroscience, New York State Psychiatric Institute, New York, NY 10032, USA

[3]Department of Neuroscience, Mortimer B. Zuckerman Mind Brain Behavior Institute, Columbia University, New York, NY 10027, USA

[4]Columbia College, New York, NY 10027, USA

[5]Lead contact

SUMMARY

During exploration, animals form an internal map of an environment by combining information about landmarks and the animal's movement, a process that depends on the hippocampus. The dentate gyrus (DG) is the first stage of the hippocampal circuit where self-motion ("where") and sensory cue information ("what") are integrated, but it remains unknown how DG neurons encode this information during cognitive map formation. Using two-photon calcium imaging in mice running on a treadmill along with online cue manipulation, we identify robust sensory cue responses in DG granule cells. Cue cell responses are stable, stimulus-specific, and accompanied by inhibition of nearby neurons. This demonstrates the existence of "cue cells" in addition to better characterized "place cells" in the DG. We hypothesize that the DG supports parallel channels of spatial and non-spatial information that contribute distinctly to downstream computations and affect roles of the DG in spatial navigation and episodic memory.

Graphical Abstract

*Correspondence: rh95@cumc.columbia.edu (R.H.), col8@cumc.columbia.edu (C.O.L.).

AUTHOR CONTRIBUTIONS

Conceptualization, C.O.L., S.N.T., and R.H.; methodology, C.O.L., S.N.T., and A.S.; software, C.O.L., S.N.T., A.D.G., and J.C.B.; formal analysis, S.N.T. and C.O.L.; investigation, C.O.L. and S.N.T.; resources, C.O.L., A.D.G., G.F.T., J.C.B., A.L., and G.O.; writing – Review & Editing, S.N.T., C.O.L., R.H., A.D.G., and A.L.; supervision, R.H and A.L.

SUPPLEMENTAL INFORMATION

Supplemental information can be found online at https://doi.org/10.1016/j.celrep.2021.110257.

DECLARATION OF INTERESTS

The authors declare no competing interests.

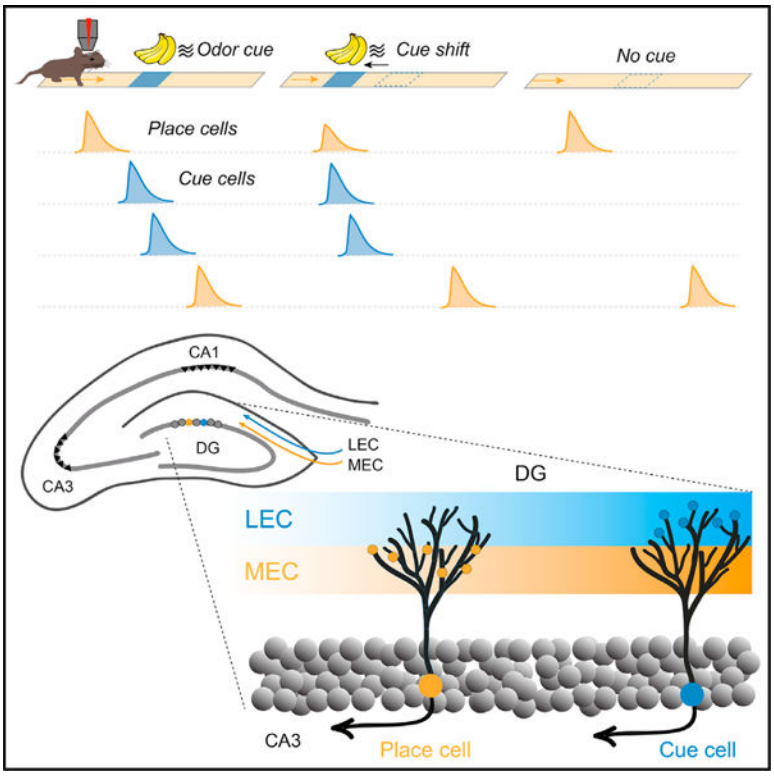

In brief

Tuncdemir et al. describe how information about spatial landmarks and movement is encoded in the first stage of the hippocampus, the dentate gyrus. The authors show that, rather than being a simple population of “place cells,” the dentate gyrus is also prominently characterized by “cue cells” independent of location.

INTRODUCTION

An animal’s location in an environment is highly relevant for guiding its behavior, both to find areas of potential reward and avoid areas of possible danger. The mammalian hippocampal formation plays a cardinal role in navigation and spatial memory by integrating self-motion and sensory cue information into a cognitive map of an environment, exemplified by the presence of “place cells” selective for specific locations within space (O’Keefe and Dostrovsky, 1971). As the initial stage in the “trisynaptic circuit” (Amaral et al., 2007), the dentate gyrus (DG) is the first region in the hippocampus to integrate sensory and self-motion information into a discrete spatial representation and thus represents the most basic state of spatial map formation (Kesner, 2013; Lee and Jung, 2017). However, causal evidence of conjunctive encoding of sensory and spatial information by the principal neurons of the DG, granule cells, is still lacking. Although recent studies have shown that granule cells may be activated by visual (Hainmueller and Bartos, 2018; Lee et al., 2009), tactile (Jung et al., 2019), and olfactory cues (Woods et al., 2020), their relationship to canonical “place cells” and their influence on spatial map formation in the DG have not been investigated.

The DG receives its main long-range excitatory inputs from the lateral and medial entorhinal cortices (LEC and MEC, respectively) and sends mossy fiber projections only to area CA3 (Witter, 2007). The LEC is thought to primarily represent information about sensory cues, whereas the MEC is thought to more prominently encode self-motion information (Hargreaves et al., 2005; Knierim et al., 2014). Because individual granule cell dendrites receive projections from both of these areas, these inputs have the potential to be the basis for dendritic computations that combine sensory and self-motion information into a discrete spatial representation (Kim et al., 2018; Krueppel et al., 2011; McNaughton et al., 1978). In concert with a highly effective winner-take-all process mediated by lateral inhibition (de Almeida et al., 2009; Marr, 1971; Treves and Rolls, 1994), these conjunctive representations could facilitate behavioral discrimination of nearby salient locations with high spatial resolution (Hunsaker et al., 2008; Lee et al., 2009). Such processes may underlie proposed computational roles of the DG in hippocampal information processing, such as pattern separation, where similar inputs are represented distinctly within the population to aid the selectivity of spatial behavior and memory (Knierim and Neunuebel, 2016; Marr, 1971).

We sought to examine how the DG participates in spatial map formation by recording calcium activity in large populations of granule cells in the mouse dorsal DG during head-fixed locomotion on a treadmill. By controlling the administration of sensory cues and their pairing with the animal's position on the treadmill, we were able to dissect sensory and spatial contributions to granule cell firing. We found that, surprisingly, most of the task-associated neurons were highly sensitive to specific sensory cues presented along the treadmill belt rather than discrete locations. Cue responses in single neurons were stable for long periods of time, sensory modality selective, and led to inhibition of other active neurons. At the same time, a smaller fraction of neurons exhibited robust spatial tuning independent of local cue presentation but were more context selective. These two channels of information, sensory and spatial, were largely distinct within the granule cell population and led us to postulate the existence of "cue cells" in addition to the better characterized "place cells" of the region. This work suggests that the DG maintains a largely separate code for cues in an environment and their location but displays specific points of integration; for example, through mutual inhibition and spatial modulation of cue response amplitudes. These properties of the heterogeneous population of cue cells and place cells may play a role in higher-level functions of the DG, such as pattern separation and contextual encoding in spatial navigation.

RESULTS

Granule cell cue responses

To investigate the interaction between sensory and spatial representations in the DG, we recorded the activity of large populations of granule cells using two-photon calcium imaging in head-restrained mice running on a treadmill (Figure 1A; Danielson et al., 2016). After habituation to head fixation, mice were trained to run to receive randomly delivered water rewards on a 2-m-long treadmill belt during 15-min sessions (Figure 1B; STAR Methods). Following initial training on the treadmill, we introduced a 1-to 2-s odor pulse delivered

in the middle of the track (90-to 110-cm position) on each lap as a dynamic spatial cue, in addition to an invariant tactile cue at the lap boundary (Figures S1A and S1B), during two-photon imaging. In this paradigm, spatial location was defined with reference to the lap boundary cue and based on locomotion of the animal since that cue, which defined the spatiotemporal relationships between events experienced by the mouse during the task. We found that the majority of spatially selective neurons exhibited receptive fields near the lap boundary and middle locations, corresponding to the lap cue and middle cue positions, respectively (Figure 1C; 57% of cells with peak activity within 10 cm of cues, 43% more than 10 cm from cues, $p = 3.5 \times 10^{-45}$, rank-sum test). To normalize locomotion-dependent modulation of hippocampal activity (Fuhrmann et al., 2015; Terrazas et al., 2005), the treadmill was motorized at a constant speed (motorized velocity, 10.11 ± 0.64 cm/s; self-driven velocity, 12.76 ± 2.45 cm/s; $p = 0.13$, Mann-Whitney test), which did not significantly alter the representation of sensory cue information in the DG compared with self-driven motion (Figures S1D–S1G).

Neurons responding reliably at cue locations could, however, be place cells that are enriched at the locations of salient stimuli, as has been suggested for area CA1 (Bourboulou et al., 2019; Hetherington and Shapiro, 1997; Hollup et al., 2001; O'Keefe and Conway, 1978; O'Keefe and Krupic, 2021; Wiener et al., 1989), or, alternately, could be directly driven by the stimulus (Woods et al., 2020). To dissociate granule cell cue responses from spatial responses, the olfactory cue was omitted or shifted one quarter of the track length (50 cm) once every 3–5 laps interleaved throughout the session (41 ± 2 laps/session). Under these conditions, a majority of neurons normally active in the middle of the track shifted their firing position to match the new location of the odor in cue-shift laps (Figure 1D, center; 79.07% ± 2.76%) and exhibited reduced activity in cue-omitted laps (Figure 1D, right; 78.2% ± 3.87%) compared with normal middle cue laps ($n = 285$ spatially tuned neurons from 8 mice). In contrast, neurons firing at locations corresponding to the invariant lap cue were unchanged in omit and shift laps. Furthermore, these cue manipulations did not result in changes in the overall spatial representation of the track by other neurons not immediately affected by the odor cue (Figure S1C). On trials with a shifted middle cue, average firing rates were higher within the new cue region (Figure 1E, red, inset; $p = 0.023$, signed-rank test; Table S1) and lower at the normal cue location on cue-omitted trials (Figure 1E, blue, inset; $p = 2.0 \times 10^{-5}$, signed-rank test) compared with the same positions during normal trials. Similar properties of DG cue responses were also seen in mice during self-driven locomotion on the treadmill (Figures S1D and S1E). Thus, a substantial population of spatially tuned DG neurons in the virtual linear track environment are, in fact, active directly in response to presentation of cues at those locations rather than the locations themselves.

Comparable population activity was found in response to cues of other sensory modalities, such as visual or tactile cues (Figures S2A–S2D), as well for liquid rewards (Figures S2E–S2H), indicating strong representation of diverse sensory variables in the DG. In addition, increasing the complexity of the environment with two additional cues at other track locations resulted in an additive pattern of single cue responses (Figures S2I–S2K), suggesting that cue activity at different locations is relatively independent and that strong cue responses are not limited to situations with a single cue alone. Cue responses were also similar for cells imaged in the dorsal DG of a granule-cell-specific transgenic

mouse (Dock10 Cre; Kohara et al., 2014; Figures S3A–S3D), indicating that sensory cue representations are indeed a property of the granule cell population rather than arising from other local neuron types, such as mossy cells or inhibitory interneurons (Jung et al., 2019).

Next we divided the spatially tuned population of granule cells into three groups for subsequent analyses based on the position of their spatial fields and their activity during cue manipulation (omit or shift) trials. The three response types are illustrated for one session: (1) cells with spatial fields within the middle cue region that closely track the changes in cue presentation ("odor-cue cells"; Figure 1F, left; STAR Methods), (2) cells with spatial fields around the lap boundary cue on the treadmill belt ("lap-cue cells"; Figure 1F, center), and (3) the remaining spatially tuned cells with receptive fields outside of the cue locations throughout the track ("place cells"; Figure 1F, right). These three groups–odor-cue, lap-cue, and place cells–constituted 22.5% ± 2%, 47.1% ± 2%, and 30.4% ± 1% of the spatially tuned cells within the imaging field of view, respectively (Figure S3E). We found that cells with similar response types did not appear to cluster together spatially within the imaging field, and the groups did not exhibit significant differences in overall mean firing rates (Figures S3E–S3G). Spatial coding properties, however, differed between cue-and place-coding populations of granule cells. Both populations of cue cells (lap and olfactory cue) showed higher average spatial information (Skaggs et al., 1993; Figure 1G; $p = 2.9 \times 10^{-11}$, Kruskal-Wallis test; STAR Methods) and had more consistent spatial firing between the first and the second half of each session than place cells (Figure 1H; $p = 3.5 \times 10^{-22}$, Kruskal-Wallis test).

To probe the emergence of receptive fields in these populations, we identified the lap in which responses began to occur within the eventual preferred spatial location of each cell during the first session of exposure to the odor cue (field onset lap; Sheffield et al., 2017; STAR Methods). We found that spatial fields in the majority of odor and lap cue cells appeared within the first 5 laps, whereas most place cell fields emerged later in the session (Figure 1I; $p = 0.0096$, Kruskal-Wallis test). In agreement with the later emergence of place cells, we found that the in-field firing rates of place cells were significantly lower than those of odor and lap cue cells only within the first 5 laps (Figure 1I, inset; two-way ANOVA, main effect of cell type: $F_{2,1473} = 6.73$, $p = 0.0012$; cell type × lap number interaction: $F_{4,1473} = 2.44$, $p = 0.04$). Cue responses were weak or nonexistent during the first cue presentation, however, and the majority of "future" odor cue cells were inactive or had low spatial tuning on an uncued treadmill belt prior to cue sessions (Figure S4), suggesting that cue cells rapidly emerge *de novo* and are not place cells that remap to new cue locations. These results demonstrate that sensory cue representations are more reliable, appear with less exposure than place cell representations, and arise from a distinct population of granule cells.

We then directly compared the odor cue cell responses in mice running on a motorized treadmill at a constant speed with responses from the same cells on a self-driven treadmill in consecutive sessions (Figure 2A). Despite notable differences in locomotion at the cue location under the two conditions (Figure S1C), the same cells fired reliably to the olfactory cue. Correlations in the spatial firing rates of individual cells show that, although both groups of cue cells were tuned similarly between self-driven and motorized

treadmill conditions, place cells were significantly less consistent in sessions with different locomotion behaviors (Figure 2B; $p = 0.0067$, Kruskal-Wallis test; Table S1), and population vector correlations were highest at cue locations (Figure 2C). We also investigated the latency of Ca^{2+} responses in sessions where the treadmill was motorized at different velocities for each lap (Figure 2D). If the cue cells were tracking the period from one cue delivery to the next, then cue-triggered response latencies would be proportional to the time it takes for the animal to traverse a lap, whereas position-triggered response latencies would be constant. On the contrary, we found shorter response latencies from a constant position when the treadmill was motorized at higher velocities and vice versa, with constant cue-triggered Ca^{2+} response latencies regardless of the velocity of the animal (Figures 2E, 2F, S1J, and S1K). These experiments demonstrate that sensory cue responses occur independent of volitional locomotion and that cue cells are not, for instance, “time cells.” Furthermore, the differing responses of cue and place cells under these conditions supports our previous findings that these are separate, dissociable populations of granule cells in the DG.

Stability and specificity of sensory cue responses

To further characterize the stability and coding specificity among the granule cell subpopulations, we investigated the responses of individual neurons over time and with respect to different sensory cues (Figures 3A and 3B). We tracked cells over multiple sessions (Sheintuch et al., 2017) and were able to find substantial numbers of the same cells active in different sessions within a day or 1 week later in the same fields of view (Figures S5A–S5G).

Between any two sessions, over days or with different cue modalities, the cells that encoded the invariant lap cue were the largest fraction of cells that remained active and maintained their response type (e.g., cue type and/or place; Figure 3C). Odor cue cells fired reliably to the same olfactory cue over long periods of time but were largely unresponsive to cues of other modalities presented at the same position ($p = 4.1 \times 10^{-6}$, Kruskal-Wallis test; Table S1). onversely, a lower percentage of place cells maintained their response type across days compared with cue cells ($p = 0.0008$, Kruskal-Wallis test). Furthermore, when we specifically examined whether cue cells become place cells between these sessions or vice versa, we found that categorical cue and place representations remain extremely stable within the DG population (Figure 3D).

We also examined the degree of stability and specificity of cue and place cell tuning by cross-correlating spatial firing rates for individual registered cells (Figure 3E). We observed that middle location odor cue cells displayed significantly lower correlations in sessions with a different sensory cue compared with separate sessions using the same olfactory cue on the same day or 1 week later ($p = 8.7 \times 10^{-7}$, Kruskal Wallis test). Thus, cells that responded to a cue of one modality were unlikely to respond to cues of other modalities despite a similar spatial location of the cues. Correlations in the activity of individual place cells over 1 week were significantly lower than on the same day and were lower than both cue cell populations, again indicating lower stability for place than cue representations ($p = 8.3 \times$

10^{-5}, Kruskal Wallis test). Notably, cells responsive to the invariant lap cue were especially stable (Figure 3E, right).

Responses of individual odor cue cells were also highly correlated between sessions recorded in different rooms on the same day (Figures 3F–3H and S5H), indicating that ambient contextual cues have a limited influence on the stability of sensory cue representation in granule cells. Despite the high stability of cue cells, place cells were significantly less consistent between rooms than cue cells in the same sessions (Figures 3G and 3H; $p = 0.0004$, Kruskal-Wallis test) and were similar to that seen in place cells over 1 week when measured in the same room (Figure 3E), suggesting that place cells are more context selective than cue cells. Furthermore, cross-registered place cells did not become cue cells in the other room and vice versa (Figure 3I; $p = 0.0025$, rank-sum test). These results suggest that sensory cues are represented by a stable subpopulation of neurons that is highly selective for specific cues, whereas purely spatial representations are less stable and undergo progressive reorganization over time and in different global contexts. It should be noted, however, that cue cells could become less stable with more drastic differences in contextual features within the rooms (for example, with differing ambient olfactory cues; GoodSmith et al., 2017; Senzai and Buzsáki, 2017), a possibility we did not fully examine.

Spatial modulation of DG cue responses

The juxtaposition of inputs from the LEC and MEC onto the dendrites of individual granule cells has been hypothesized to underlie a conjunctive code for sensory cues and their spatial location (Kesner, 2013; Lee and Jung, 2017). We therefore examined the influence of spatial location on cue responses (“spatial modulation”) by tracking odor cue cells through multiple sessions with different cue-location pairings, either with an intermittently shifted cue as in previous experiments or in separate sessions with the same cue at random locations for each lap (Figures 4A and 4B). On average, cue-triggered Ca^{2+} response amplitudes for individual cue cells were smaller when cues were presented at the infrequent “shift” location or at random locations compared with their responses at the more frequent middle location (Figures 4C and 4D; $p = 5.5 \times 10^{-6}$, Friedman test; Table S1). Thus, although cue cells tend to respond to the same sensory cue regardless of location, the strongest responses occur when a cue is presented repeatedly at the same place.

To further examine the spatial modulation of cue responses, we delivered a visual cue at multiple locations on the track to measure the selectivity of granule cell responses to cues presented consistently at distinct locations (“dual location cue”; Figure 4E; Saleem et al., 2018; Zhao et al., 2020). Again, each cue was omitted on a subset of laps to isolate cue cells as opposed to place cells present in the vicinity of cues (Figures S6A and S6B). To measure the extent of preference for one cue location versus the other, we calculated the spatial modulation index for each cue cell as the ratio of the firing rate in the non-preferred cue location versus the preferred cue location. Cue cells in the first session were modulated significantly by the cue location ($p = 1.6 \times 10^{-9}$, signed rank test on day 1, with 53% of cells significantly spatially modulated; Figure 4F; STAR Methods); however, spatial modulation also increased over several days of dual cue presentations ($p = 0.013$ rank-sum test, day 1 versus day 2, 3, or 4), with 81% of cue cells exhibiting significant spatial modulation by

day 4 (Figures 4G, 4H, S6C, and S6D). This suggests that dentate cue cells are modulated acutely by the spatial location of two identical cues but increase their preference for a single location over days.

Effects of cue manipulation on spatial encoding in the DG

Although the most robust activity in the DG was found within the cue cell population, the existence of the smaller population of place cells in uncued locations suggests that spatial activity in these cells is referenced to one of the two cues on the otherwise featureless treadmill track to encode a unique location. We therefore examined the effect of manipulations of the variable cue on the subsequent spatial encoding of place cells to judge the degree to which this cue acts as a landmark. For example, if place cells were referenced to the nearest cue, then we would expect the receptive fields of all place cells following the variable middle cue to shift on cue-shifted laps. We first calculated population vector (PV) correlations of firing rates across all spatially tuned cells (cue and place cells) on normal and cue-shifted laps (Figure 5A). Although the correlation was higher in the vicinity of the cues between normal laps, we observed a dramatic decrease in PV correlation between normal and cue-shifted laps that was confined to the area immediately around the middle cue. However, this change in PV correlation did not extend much beyond the cue location, consistent with a limited effect of cue shifting on subsequent place cell activity.

To further evaluate the manner in which cue-associated activity contributes to spatial encoding, a spatial Bayesian decoder was constructed from the firing rate vectors of all spatially tuned cells (Grosmark and Buzsáki, 2016; 4,091 cells from 66 sessions, n = 8 mice) and tested on normal laps or laps with a shift or omission of the middle cue (Figure 5B). Decoder accuracy was higher in normal (median, 10.6 cm) compared with cue-shifted (median, 19.6 cm) and cue-omitted laps (median, 18.4 cm, $p = 1.8 \times 10^{-6}$, signed-rank test; Figure 5C; Table S1; data not shown for omit laps), indicating that cue manipulations affect the accuracy of spatial coding by the DG population. However, although the cue shift strongly perturbed spatial decoding near the shifted cue, estimating the animal's position to be farther along than the real position, the decoder error on shift laps soon converged to that of normal laps, well before the subsequent lap cue (Figure 5D, dotted line). These results suggest that the spatial encoding of granule cells is affected by sensory cues only within a localized area near the cues rather than persistently altering their estimation of the animal's position like a landmark.

We next examined responses of individual granule cells by measuring cross-correlation offsets between spatial firing in normal and cue-shifted laps for each cell and found two distinct classes of single-cell shift responses: some cells shifted their firing precisely along with the odor cue shift distance (0.5 m), whereas others were consistently referenced to the stable lap boundary cue and did not shift their response location during the odor cue location shift (Figures 5E and 5F). The majority of cells that shifted their firing in reference to the new cue location were active immediately in response to the middle cue ("middle cue influenced"), whereas a small number was persistently affected by the cue shift. In contrast, a relatively constant number of place cells along the track maintained their normal firing location with reference to the distant lap boundary cue despite the shifted local cue

("non-middle cue influenced"). Notably, there was also a small enrichment of place cells immediately prior to the cue but unaffected by the cue shift (Figure 5F), indicating a spatial response predictive of the normal cue location. The presence of two distinct groups of cells that fire in reference to the two cues on the treadmill track (the variable middle cue and stable lap cue) suggests that the DG population maintains independent spatial reference frames based on distinct cues within an environment. This code, however, appears to differ depending on the spatial stability of the cues; the effects of spatially variable cues are limited to the cue cell population, whereas place cells are referenced to global landmarks (Wang et al., 2019).

Cue-related inhibition of GC firing

Spatial receptive fields of granule cells are hypothesized to form within a competitive network in which lateral inhibition mediated by GABAergic interneurons enforces sparse encoding that may aid pattern separation (de Almeida et al., 2009). The robust and highly selective cue responses of granule cells in our behavioral paradigm allowed us to examine patterns of local-circuit inhibition within the DG network. First we sought to analyze the effect of cue responses on spontaneous firing observed within the spatially tuned granule cell population. By comparing spontaneous ("out of field") firing rates at the middle cue location in normal laps with laps where the cue is omitted, we identified a significant reduction in spontaneous firing of the granule cell population during cue presentation (Figure 6A; $p = 0.0004$, signed rank test; Table S1), which was absent on cue-omitted laps and co-varied with the mean amplitude of cue-related excitation ("within field"; Figure 6C). Furthermore, the timing of the peak of this inhibition was delayed with respect to the excitatory cue response in these sessions (Figures S6E and S6F). These data show that sensory cue input is able to suppress "noisy" spontaneous firing in the granule cell population, potentially through lateral inhibition.

In addition to suppressing spontaneous firing in the DG network, we sought to determine the effect of cue responses on activity in the place cell population and in cells responding to other cues. By examining cells with receptive fields normally at the intermittent shift location, we found that place cell firing rates were strongly suppressed on shift laps when a cue was presented at this location compared with normal laps when a cue was not present here (Figures 6D and 6E). Furthermore, when two distinct cues were normally presented at different locations, intermittent shifting of the position of one cue to overlap with the other cue typically had the effect of suppressing the responses in both cue populations (Figures 6F and 6G), indicating mutual inhibition among granule cells encoding different cues. Thus, in addition to inhibition of spontaneous firing in the granule cell population, cue responses lead to overall inhibition of place cell responses and responses to competing cues as well. Our results suggest that cue-related activity in granule cells and the resulting suppression of responses in neighboring cells via lateral inhibition may form a competitive network that utilizes the strongest and perhaps the most informative parameters, such as stable landmark cues, to accurately establish an animal's location in space.

DISCUSSION

By imaging calcium activity in large populations of dentate granule cells during head-fixed spatial behavior on a treadmill, we showed that a major population of task-selective neurons is highly sensitive to specific sensory cues (non-spatial or “what” information) rather than to discrete locations (spatial or “where” information). The ability to dynamically manipulate a sensory cue and its association with locations on the treadmill track allowed us to isolate the population of cue cells in addition to the complementary population of place cells recorded in the same sessions.

The robust and consistent nature of GC cue responses suggests that cue-selective populations may have been similarly present in prior experiments recording DG activity *in vivo*, but the lack of precise stimulus control made it impossible to distinguish cue-responsive versus place-responsive components (Hainmueller and Bartos, 2018; Jung et al., 2019; Leutgeb et al., 2007; O’Keefe and Krupic, 2021). A major effect of sensory cues on DG firing largely independent of spatial context might also explain the relatively lower context selectivity observed in the DG compared with other hippocampal subfields, at least when measured in different contexts that contain the same or similar sensory cues (Good-Smith et al., 2017; Hainmueller and Bartos, 2018; Leutgeb et al., 2007; Senzai and Buzsáki, 2017). To support this notion, we found that DG cue cells were largely stable when recorded over long periods of time, with different cue positions and locomotion speeds or in different room contexts, whereas place cells were not (Figures 2, 3, and 4).

Origin of cue and place responses in the DG

Previous work has demonstrated that the two major long-range inputs to the DG, the LEC and MEC, are involved in processing functionally distinct information (Hargreaves et al., 2005; Knierim et al., 2014). This raises the possibility that our “cue cells” may be driven primarily by sensory inputs from the LEC, whereas “place cells” are driven by self-motion information relayed from the MEC. The segregation of these properties within the overall granule cell population suggests that these streams of information remain largely separated at the level of the DG (Fernández-Ruiz et al., 2021), similar to the functional heterogeneity observed in other hippocampal subfields (Cembrowski and Spruston, 2019; Soltesz and Losonczy, 2018). In these regions, such heterogeneity among principal neurons has been hypothesized to be critical for efficient encoding of spatial representations (Cembrowski and Spruston, 2019; Chelaru and Dragoi, 2008; Fernández-Ruiz et al., 2021; Soltesz and Losonczy, 2018). Heterogeneity has also been observed in immediate-early gene expression profiles within DG neurons encoding individual memory engrams (Sun et al., 2020), which are targeted differentially by entorhinal afferent pathways (Erwin et al., 2020; Luna et al., 2019; Sun et al., 2020; Witter, 2007). These findings are in line with our study demonstrating that sensory and spatial information remain partially separate at the level of the DG and suggest that multiple channels of spatial and non-spatial information contribute distinctly to local and downstream computations. This separation is also consistent with the idea that cue-based and path integration-based navigation are complementary rather than integrated to produce place-specific firing in locations where landmark cues are present as well as in between cues (Poucet et al., 2014).

Limitations of the study

It is possible that, rather than encoding non-spatial “what” information (O’Keefe and Krupic, 2021), “cue cells” in our study could actually be place cells encoding “where” information within a different reference frame (van Dijk and Fenton, 2018; Radvansky et al., 2021). However, we observed robust responses in the same cue cells even to an odor cue administered randomly in each lap (Figures 4A–4C). This suggests that a global reference frame is not necessary for cue responses. However, responses did seem larger for cues presented at a regular spatial location (Figure 4C) and for the lap cue, which is the most consistent and frequent feature during individual sessions and across the entire experimental timeline and also appears to more strongly influence the firing of place cells (Figures 5D and 5E). It is therefore likely that two distinct cues (e.g., odor and lap cues) presented consistently at a different spatial frequency may indeed produce independent populations of associated place cells referenced to these landmarks. Regardless, our results strongly suggest that non-spatial rather than purely space-related information is carried by the population of cue cells.

Furthermore, although different from previous studies (Danielson et al., 2016, 2017; Hainmueller and Bartos, 2018; Jung et al., 2019), motorizing the treadmill does not affect our central claim of the strong representation of sensory cue information in the DG (Figures 2 and S1). Running on motorized treadmills also does not influence the differences in the stability and tuning properties between the cue-and place-encoding populations (Figures 1 and S1). However, we note that these differences observed during head-fixed navigation on a relatively cue-impoverished track at a constant speed may be larger than what would be observed during self-guided exploration of cue-rich, multisensory, real-world environments. Future studies investigating whether cue- and place-encoding populations receive different inputs from the LEC and MEC as well as the molecular basis of the heterogeneity among granule cell populations will allow a more detailed inquiry into the functional diversity in DG granule cells. Such studies may also allow us to selectively target cue and place cells to manipulate their activity and determine their roles during discrimination behaviors.

Functional significance of DG cue cell properties

Our results show that individual granule cells respond to the same cues when presented in different locations, but the strength of this activity is spatially modulated (Figures 4 and S6). This indicates that spatial information is present in some form within the cue cell population, and, thus, cue and spatial channels of information are not entirely separate. However, the incremental modulation we observed is quite different from a strict requirement for pairing of cue and spatial input that would lead different cells to fire to the same stimuli when presented at different locations. Thus, the spatial modulation of cue responses we observed in the DG more closely resembles “rate remapping” documented previously documented in the region versus “global remapping” ascribed to area CA3 (Leutgeb et al., 2007). However, differential encoding of cues based on their spatial location may still contribute to pattern separation in the hippocampus by allowing discrimination between similar cues in downstream areas. We also observed that cue responses are more robust for stimuli paired repeatedly with one particular location, such as our invariant lap cue, and that spatial modulation increases with experience, which may indicate plasticity in dendritic

integration of sensory and spatial information. Although, in all of these cases, the influence of space on cue responses is incremental, conjunctive encoding of sensory cues and their locations within an environment through rate modulation could play a role in establishing landmarks for spatial navigation (Tuncdemir et al., 2019). Furthermore, the sensitivity of DG place cells to time and context could indicate a role for this less stable population in contextual encoding, a function ascribed previously to the DG related to pattern separation (Hainmueller and Bartos, 2018; Maurer and Nadel, 2021; McHugh et al., 2007).

Previous work has shown that CA regions also have cue responses (Bourboulou et al., 2019; Hetherington and Shapiro, 1997; Hollup et al., 2001; O'Keefe and Conway, 1978; Wiener et al., 1989), but all of these areas receive direct (CA3) or indirect input (CA1) from the DG as well as the entorhinal cortex, so it remains unclear whether these properties arise as a result of direct inputs from entorhinal regions or through the hippocampal trisynaptic circuit. Thus, the DG is the ideal place to look at how channels of information from the LEC and MEC are initially integrated by the hippocampus during spatial map formation. Our work suggests that the DG encodes representations of sensory cues in the environment that interact weakly with spatial representations (Figure 4), potentially through lateral inhibition (Figure 6) or cue-related suppression in upstream areas, including the entorhinal cortex. This is consistent with the hypothesis of a competitive network in the DG enforced by strong lateral inhibition, which has been suggested to contribute to pattern separation. The rate-modulated code of DG sensory cue representations could then be further refined in subsequent hippocampal areas such as the CA3 recurrent attractor network. These circuits may resolve incomplete or conflicting cue and path integration-based information from the DG to estimate an animal's position within an integrated spatial map. Future studies examining how these specific features manifest in subsequent stages of the hippocampal circuit will shed light on the progressive hippocampal processing and integration of sensory cue and spatial information.

The properties of cue and place cells in the DG have the hallmark of features one might expect from the first stage of spatial map formation in the hippocampus: mostly distinct but slightly mixed encoding of sensory cues (or "what") and place (or "where"). Such complementary channels of information may be refined by downstream hippocampal areas into an integrated spatial map that encodes relationships between important features such as spatial cues and goals, which can be used to organize adaptive behavior. Uncovering the functional heterogeneity of cue and place cells in the DG helps us to better understand the basic neural mechanisms underlying our ability to navigate in complex environments by utilizing both landmarks and self-motion information to guide our movements through space.

STAR★METHODS

RESOURCE AVAILABILITY

Lead contact—Further information and requests for resources and reagents should be directed to and will be fulfilled upon request by the lead contact, Rene Hen (rh95@cumc.columbia.edu).

Materials availability—This study did not generate new unique reagents.

Data and code availability

- All data reported in this paper will be shared by the lead contact upon request.
- All original code has been deposited at github.com/claylacefield/TuncdemirHenLacefield-CellReports2021 and is publicly available as of the date of publication. DOIs are listed in the key resources table.
- Any additional information required to reanalyze the data reported in this paper is available from the Lead Contact upon request.

EXPERIMENTAL MODELS AND SUBJECT DETAILS

Mice—All procedures were conducted in accordance with the U.S. NIH Guide for the Care and Use of Laboratory Animals and the Institutional Animal Care and Use Committees of New York State Psychiatric Institute and Columbia University. Adult male C57BL/6J mice were supplied by Jackson Laboratory and Dock10^{Cre} mice were a gift from Susumu Tonegawa (Massachusetts Institute of Technology). Mice were housed in a vivarium grouped 2–4 mice/cage enriched with running wheels, maintained on a 12-hour light cycle and used at 8–10 weeks of age. Experiments were conducted during the light portion of the cycle. Food and water were available *ad libitum* until the beginning of the experiment, when they were placed under controlled water supply and maintained at >90% of their pre-deprivation weight over the course of imaging experiments. In total, imaging data from 18 mice were used in this study.

METHOD DETAILS

Surgery—Dentate gyrus virus injection and imaging window implantation surgeries were performed as described previously (Danielson et al., 2016, 2017). For all surgical procedures, mice were anesthetized with 1.5% isoflurane at an oxygen flow rate of 1 L/min, and head-fixed in a stereotactic frame (Kopf Instruments, Tujunga, CA). Eyes were lubricated with an ophthalmic ointment, and body temperature maintained at 37°C with a warm water recirculator (Stryker, Kalamazoo, MI). The fur was shaved and incision site sterilized prior to beginning surgical procedures, and subcutaneous saline and carpofen were provided peri-operatively and for 3 days post-operatively to prevent dehydration and for analgesia. Mice were unilaterally injected with recombinant adeno-associated virus (rAVV) carrying the GCaMP6s transgene (pAAV.Syn.GCaMP6s.WPRE.SV40) purchased from Addgene (viral prep #100843-AAV1) with titer of 1–5×10^{12} in dorsal dentate gyrus using a Nanoject syringe (Drummond Scientific, Broomall, PA). Injection coordinates were −2 mm AP, −1.5 mm ML, and −1.85, −1.7, −1.55 mm DV relative to the cortical surface. 30 nL of diluted virus was injected at each DV location in 10 nL increments. Mice were allowed to recover for 3 days and then were unilaterally implanted with an imaging window and stainless steel head-post for head fixation. Imaging windows were constructed by adhering 2 mm diameter, 2.3 mm long stainless steel hypodermic tubing (Ziggy's Tubes and Wires Inc, Pleasant Hill, TN) to 2 mm diameter glass coverslips (Potomac Photonics, Halethorpe, MD). A 2 mm diameter craniotomy was made centered on the previous injection site with a taper pointed-drill (Henry Schein Inc, 9004367) and dura was removed with micro curette (FST, 10080–05). The overlying cortex was gently

aspirated to reveal capsular fibers with continuous irrigation with ice cold aCSF solution and bleeding was controlled with a collagen gel sponge (Avitene). Under minimal bleeding, a 30 g blunt syringe was used to gently aspirate capsular and CA1 alveus fibers with white appearance and CA1 pyramidale and moleculare with pink appearance until vasculature of the hippocampal fissure became visible (under bright light with low bleeding). The cannula, attached to the stereotactic handle, was then gently lowered into the craniotomy and affixed to the skull using dental cement (Unifast Trad powder and LC light cured acrylic UV, Henry Schein).

Behavioral training and apparatus—After a minimum of 1 week recovery period, mice underwent a water restriction scheme (1 ml per day) and trained to run on treadmill while head-restrained. The training period typically lasted a week (2 training sessions/day, 15 min each) until the mice were able to run for at least 1 lap/ minute and seek reward from one of 3 reward zones that were randomly selected along the belt on each traversal by licking the water delivery port. We then initiated the motorized belt adjusted to the natural velocity of each mouse and proceeded training for 1–2 more days. We discarded mice that did not perform sufficiently to receive getting all of their daily water supply during treadmill training, and were not motivated to move on the treadmill. A separate cohort of mice ran at will on the treadmill (Figures 2 and S1). During the training period mice ran on a cue-less ‘burlap’ belt and progressed to a different belt containing cues of different modalities as described below. For room switch experiments (Figures 3F–3H), mice were transferred to a separate room with similar imaging equipment on another floor of the building in their home cage. Mice were imaged for two consecutive sessions/day, each 15 minutes long, for the duration of 7–10 days. Single odor, light, and whisker texture responses described in Figures 1, 3, and S2–S5 are from the first time mice were exposed to these sensory stimuli. The subsequent exposures to these sensory cues, they were either in different locations on the belt, preceded or followed by additional cues (Figures 4 and 6), reducing the effects of learning the location of these cues. Additionally, in all experiments, the treadmill belt material was changed between sessions to reduce the chances of urine contamination which might act as an additional olfactory cue.

The behavioral apparatus consisted of 2 m long, 3” wide cotton fabric belt stretched between 6” diam. laser-cut plastic wheels, mounted on an aluminum frame (8020.net). Spatial triggering of task events was performed by custom software via serial communication with a microcontroller (Arduino DUE) and an associated printed circuit board (OpenMaze OM4 PCB, www.openmaze.org) on the treadmill. The axle of the treadmill wheel was attached to a quadrature rotary encoder (US Digital #MA3-A10–125-B) connected to a custom quadrature decoder board and Arduino Nano (courtesy of Wen Li). Angular displacement was converted into a virtual linear distance based on the circumference of the treadmill wheels, and laps were determined by reading an RFID chip on the treadmill belt attachment point with an RFID reader (Sparkfun #ID12LA) mounted under the animal’s head fixation point (Figures S1A and S1B). A 12 V DC gear motor was attached to the axle of the treadmill connected to a separate Arduino/OpenMaze shield using pulse-width modulation to adjust the rotation speed. A water reservoir connected to a water delivery port consisting of a small gavage needle (Cadence Science) was placed within reach of the mouse’s tongue.

A capacitance touch sensor (Sparkfun MPR121) was attached to the water port to measure licking and the sensor was connected to the Arduino/OM4 PCB. Small 2–3 ml drops of water were delivered by the brief opening a solenoid valve (Parker Hannefin) connected to the water port. Rewards were triggered at random locations each lap when mice entered a 10 cm long reward zone on the track and were available until mice exited the reward zone or 3 sec had elapsed. Olfactory stimuli consisted of undiluted isoamyl acetate (IAA, Sigma W205532) which was added to syringe filters (Whatman #6888–2527) and delivered by opening a solenoid valve (SMC) connected to a flow controller delivering constant airflow of compressed medical grade air for 1s (~3psi). Visual and tactile stimulation consisted of a red LED contralateral to the imaged region, or a 1" square piece of sand paper brushed by the contralateral whiskers using a stepper motor, at approximately the speed of the treadmill belt. Custom written Be-Mate algorithm implemented in Java was used for recording mice's licking, its position on the belt, and cue delivery. Mice were monitored using an IR camera (PS3eye) and illuminated using an IR LED array.

To isolate cue-selective responses among the granule cell population, normal cue laps in which the olfactory, visual, or tactile cue was presented in the middle of the treadmill track (90–110 cm) were interspersed with occasional laps (10–20% of laps) in which the same cue was omitted ("omit" laps), or shifted forward ¼ of the track ("shift" laps, 40–60 cm cue position). For a subset of sessions, the olfactory cue was presented at one of 5 locations along the track randomly each lap, in order to examine the effect of spatial pairing of the cue.

***In vivo* two-photon imaging—**Imaging was conducted using a microscope setup which consists of 8 kHz resonant galvanometer (*Bruker*) mounted to a mirror-based multi-photon microscopy system (*Prairie Technologies*) and an ultra-fast pulsed laser beam (920-nm wavelength; *Chameleon Ultra II, Coherent*, 20–40-mW average power at the back focal plane of the objective) controlled with an electro-optical modulator (*Conoptics*, Model 302 RM). GCaMP fluorescence was excited through a 40x water immersion objective (Nikon NIR Apo, 0.8 NA, 3.5 mm WD) and fluorescence signals detected with photomultiplier tubes (*Hamamatsu 7422P-40*), acquired with PrairieView software (*Prairie*) at 30fps frame rate (512×512 pixels, 1.3 μm/pixel). A custom dual stage preamp (1.4×10^5 dB, Bruker) was used to amplify signals prior to digitization. Two goniometers (Edmund Optics) were used to adjust the angle of each mouse's head in order to achieve the same imaging plane over multiple sessions.

Data processing for Ca^{2+} imaging: Movies were motion corrected using NoRMCorre algorithm using a non-rigid registration method that splits the field of view (FOV) into overlapping patched that are registered separately then merged by smooth interpolation (Pnevmatikakis and Giovannucci, 2017). Videos were then spatially and temporally down-sampled by 2 to reduce noise and the computational power required for cell segmentation. Spatial and temporal components for individual cells were extracted using large-scale sparse non-negative matrix factorization (CNMF/CaImAn) (Giovannucci et al., 2019) or using the singular value decomposition method by Suite2p algorithm (http://github.com/cortex-lab/Suite2P), both of which resulted in similar regions of interest (ROIs). We used Suite2p

graphical user interface to manually select small, densely packed DG granule cells and discard large isolated cell bodies corresponding to mossy cells or other hilar interneurons. To obtain total number of DG granule cells within the imaging fields of view in a subset of total sessions, time averaged images were segmented using the Cellpose algorithm (https://github.com/MouseLand/cellpose) followed by manual inspection. Ca^{2+} transient events were defined by a custom detection algorithm which identifies fluorescence peaks with a rise slope greater than 4 standard deviations above an iteratively refined baseline.

Behavioral and calcium data alignment: Behavioral data were aligned to Ca^{2+} data using the record of a synchronization signal between the two computers used for data collection. Behavioral data were down-sampled to match Ca^{2+} imaging data.

Data analysis—Data were analyzed using custom-written routines implemented in MATLAB. Plots were generated in MATLAB and Prism.

Identification of spatially-tuned neurons: We restricted our analysis to continuous running at least 2 sec in duration and with a minimum peak speed of 5 cm/sec. For each lap crossing, position data and Ca^{2+} transient events for each cell were binned into 2 cm-wide windows (100 bins), generating raw vectors for occupancy-by-position and calcium transient numbers-by-position which were then circularly smoothed with a Gaussian kernel (SD = 5 cm). A firing rate-by-position vector was computed by dividing the smoothed transient number vector by the smoothed occupancy vector. Within each lap, we circularly shuffled the positions 1000 times and recomputed firing rate-by-position vectors to generate a null distribution for each spatial bin. A spatially selective cell was defined that met the following criteria: (a) the cell should fire above its mean firing rate within its spatial field in at least 20% of laps or for a minimum of 3 laps; and (b) observed firing should be above 99% of the shuffled distribution for at least 5 consecutive spatial bins (10 cm) wrapping around the two edges of the belt. We have identified spatially tuned neurons by excluding bins in which sensory cues were omitted or shifted and calculated firing rate vectors in these laps separately. Among all of the spatially tuned neurons, *"middle cue cells*" (also termed as odor-cue, light-cue or tactile-cue cells depending on the type of cue delivered in the middle of the track for analysis of data using only one type of cue) were defined as those with averaged spatial fields that overlapped with at least 50% of the 45^{th} and 55^{th} bins and had peak amplitude at least two times larger than those in cue-omitted laps. "Lap-cue cells" were defined as those with averaged spatial fields overlapping at least 50% of the region wrapping around the 90^{th} and 10^{th} bins in the normal laps and have peak amplitude in cue-omitted laps and cue shifted laps not exceeding than at least two times of that in normal laps. The remaining cells constituted the "place cells".

Spatial information, stability, consistency, and emergence of spatial fields: To calculate a measure for spatial information content for granule cells in Figure 1G, we adapted a traditional method of spatial information assessment (Danielson et al., 2016; Grosmark et al., 2021; Skaggs et al., 1993) to Ca^{2+} imaging data. For each cell, we used the firing rate-by-position vector and shuffled null distribution computed above and calculated the spatial information content (Grosmark et al., 2021; Skaggs et al., 1993) as follows:

$$\mathrm{SPE} = \sum_i p_i \frac{\lambda_i}{\lambda} \log_2 \frac{\lambda_i}{\lambda}$$

Where λ is the overall mean event rate, λ_i is the mean event rate of each cell in the i^{th} bin, p_i is the probability of that mouse being in the i^{th} bin that is occupancy in the i^{th} bin/ 15mins.

To account for the fact that low firing rates artificially produce high spatial information scores, we subtracted the mean of the shuffled information per spike from observed information per spike, divided by the standard deviation of the shuffled values to determine the spatial variance for each cell. Therefore, the amount of spatial information is inferred from differences in normalized Ca^{2+} activity in each neuron and reported as bits per seconds. The consistency of place field firing in Figure 1H was determined as the cross-correlation between the averaged firing rate-by-position vector of the first and the second halves of the total number of cue normal laps within a session. We determined place field onset lap in cue normal laps (Figure 1I) as described previously (Sheffield et al., 2017). Briefly, starting on lap 1 we searched for a significant Ca^{2+} transient event present within the boundaries of the previously determined mean spatial field calculated from all the laps in the session. If one were found we would then search for Ca^{2+} transient event on each of the next 4 laps. If 3 of the 5 laps had Ca^{2+} transients within the mean place field boundaries, lap 1 would be considered the place field onset lap. If either lap 1 had no Ca^{2+} transient or less than 3 of the 5 laps had Ca^{2+} transient, we would move to lap 2 and repeat the search (Figure 1I). The field onset laps, and the mean firing rates during first 5, 6–10 and 11–15 laps was then assessed for each group of cells.

Multi-session cell tracking: Cells were tracked across sessions using CellReg (Sheintuch et al., 2017). Briefly, rigid alignment with both translations and rotations was performed on spatial footprint projections of each session and manually inspected for quality. To improve performance with our data, we modified the CellReg source code to consider complete spatial footprints instead of centroids during alignment. The centroid distance between neighbors was then calculated and used to create a probabilistic model that estimated the expected error rate at different thresholds. The optimal centroid distance threshold was chosen by the algorithm and used to match cells. A clustering algorithm then refined these decisions previously made using pairwise comparisons.

Following cell registration, tracked cells were matched with their corresponding functional cell types (i.e. mid-, lap-cue, place cells, as described above). All analyses presented in Figure 3 are carried out pairwise, to maximize the number of cells in each comparison and to minimize the total number of comparisons. For multiday comparisons we used Day1, session 1 as the normal session, and for multisession comparisons we used Visual stimulus session as the normal session. To calculate the fraction of cells that maintain their identity, cell pairs that were counted as being the same cell type in both sessions was divided by all of that cell type in the normal session. In order to derive a null distribution for preservation of pairwise identity, we randomly permutated the cell IDs of all the tracked cells in pairwise sessions 1000 times and calculated the fraction of cells that were the same, among all of that

cell type in the normal session. We calculated p-values by comparing actual data to this null distribution, 97.5th% of the null distribution is presented dotted lines in Figure 3.

Rate correlation and population vector (PV) analysis: Comparison of the activity between different sessions was calculated using Pearson's correlation of the spatially binned, averaged firing rate-by-position vector in cue normal laps in Figures 2, 3, and S4. The variability in neural activity between self-driven and motorized treadmill sessions (Figure 2) and between lap types (in Figure 6) was calculated by using Pearson's correlation on each 2 cm bins of the firing rate-by-position vector along the treadmill during odor cue trials (mean for all spatially tuned cells).

Spatial modulation: To compare single cell cue responses at different locations, cue-triggered average z-scored calcium transients were measured for cue cells, defined with reference to omit lap activity as done previously, for middle cue sessions. For dual cue location experiments, cue cells were identified as units with receptive field peaks in the cue location whose cue-zone calcium event rate was greater than 95% of shuffled responses versus the cue-omitted laps. For statistics of spatial modulation over days, cue cells that significantly preferred one cue location were counted when responses at one location exceeded 95% of the shuffled cue position event rates. Spatial modulation in this paradigm is listed as a ratio of mean spatial firing rates for the non-preferred location over the preferred location rates for each cell (i.e. lower values correspond to higher spatial selectivity of cue responses).

Bayesian reconstruction analysis: To calculate the probability of the animal's position given a short time window of neural activity, we used a previously published method based on Bayesian reconstruction algorithm(Grosmark and Buzsáki, 2016). Briefly, Ca^{2+} transient events for each cell were binned into 1 second windows to construct firing rate vectors. For each of these binned firing rate vectors, Bayesian classification of virtual position (posterior probability for each bin) was performed by a previously described method(Grosmark and Buzsáki, 2016) utilizing a template comprising of a cell's smoothed firing rate-by-position vectors. In order to cross-validate our decoding procedure, we divided firing rate-by-position template into lap crossings, used 1/5th of laps as "testing" dataset while the remaining 4/5th of laps constituted the "training" dataset. For example, lap 1 was tested based on the firing rate-by-position vectors calculated using laps 2,3,4,5, lap as template, and lap 6 was tested based on the firing rate-by-position vectors calculated from laps 7,8,9,10, and so on. The resulting posterior probability distribution for each bin is the likelihood for an animal is located in that bin, which adds up to 1, and the bin with the maximum posterior probability is the estimated position of the animal. To determine the decoding error we calculated the absolute difference between the animal's actual position and the maximum posterior probability in that bin. Post-reconstruction, we divided the time bins (excluding those with no activity) according to the lap types.

Single cell cue shift analysis: Spatial firing rates for each spatially tuned cell on normal middle cue laps were cross-correlated with firing rates on shift laps in order to estimate the cross-correlation peak offset (i.e. shift magnitude) for each cell after cue manipulation.

Binned histograms of numbers of cells with spatial receptive fields at particular locations along the track were plotted with respect to their shift magnitudes. Numbers of cells were averaged over populations showing no shift (−5 to 5 cm shift) or that shifted their firing along with the cue (50 cm±5 cm).

Inhibition analysis: Out-of-field firing was calculated for cells found to be significantly spatially tuned on normal middle cue laps by extracting calcium event rates in the ~200 cm track length excluding the peak place field (+/− 10 cm). Average out-of-field firing rates were then calculated across all cells for cue laps and intermittent laps where the cue was omitted. For comparison of cue-associated excitation and inhibition levels, average firing rates were computed by session for the 20 cm region surrounding the middle cue, with respect to the normal pre-cue baseline firing rate. Cue-related inhibition of place cell firing was calculated by selecting spatially tuned cells whose firing field on normal middle cue laps fell within the region of the cue on shift laps (50–80 cm). Firing rates for these cells were then averaged for normal laps where the cue was not presented in this region and compared with laps where the cue was shifted to this region (50 cm). Mutual inhibition between cues was calculated by first selecting cells responsive to each of 2 cues of different modalities (olfactory or visual) presented at 40 cm and 120 cm. Responses were then averaged for each cue cell for laps in which the cues were presented alone at these locations versus intermittent laps where the cues were presented together at one of the two former locations.

QUANTIFICATION AND STATISTICAL ANALYSIS

Data were analyzed using custom software written in MATLAB 2019. All statistical parameters including mean ± SEM and statistical significance for specific analyses are reported in the text, and the Table S1 of the paper. All statistics tests were non-parametric, made no assumptions about the distribution of the data, and no statistical methods were used to predetermine sample sizes. The significance threshold was placed at $p<0.05$.

Supplementary Material

Refer to Web version on PubMed Central for supplementary material.

ACKNOWLEDGMENTS

We would like to thank Jack Berry and other members of the Hen lab for critical insights throughout this project. This work was funded by NIH K99 MH122226 (to S.N.T.), S10 OD018464 (to S.N.T. and G.F.T.), NYSTEM-C029157 (to G.O., G.F.T., C.O.L., and R.H.), a Revson Fellowship in Biomedical Science (to A.D.G.), NIMH R21MH122965 and a BBRF Young Investigator Award (to G.F.T.), NIMH R01 AG043688 and MH068542 (to R.H.), and NIMH R01 MH100631, NINDS R01NS094668, and NINDS U19NS104590 (to A.L.).

REFERENCES

Amaral DG, Scharfman HE, and Lavenex P (2007). The dentate gyrus: fundamental neuroanatomical organization (dentate gyrus for dummies). Prog. Brain Res 163, 3–22. [PubMed: 17765709]

Bourboulou R, Marti G, Michon F-X, El Feghaly E, Nouguier M, Robbe D, Koenig J, and Epsztein J (2019). Dynamic control of hippocampal spatial coding resolution by local visual cues. ELife 8, e44487. [PubMed: 30822270]

Cembrowski MS, and Spruston N (2019). Heterogeneity within classical cell types is the rule: lessons from hippocampal pyramidal neurons. Nat. Rev. Neurosci 20, 193–204. [PubMed: 30778192]

Chelaru MI, and Dragoi V (2008). Efficient coding in heterogeneous neuronal populations. Proc. Natl. Acad. Sci. U.S.A 105, 16344–16349. [PubMed: 18854413]

Danielson NB, Kaifosh P, Zaremba JD, Lovett-Barron M, Tsai J, Denny CA, Balough EM, Goldberg AR, Drew LJ, Hen R, et al. (2016). Distinct contribution of adult-born hippocampal granule cells to context encoding. Neuron 90, 101–112. [PubMed: 26971949]

Danielson NB, Turi GF, Ladow M, Chavlis S, Petrantonakis PC, Poirazi P, and Losonczy A (2017). In vivo imaging of dentate gyrus mossy cells in behaving mice. Neuron 93, 552–559.e4. [PubMed: 28132825]

de Almeida L, Idiart M, and Lisman JE (2009). The input-output transformation of the hippocampal granule cells: from grid cells to place fields. J. Neurosci 29, 7504–7512. [PubMed: 19515918]

Erwin SR, Sun W, Copeland M, Lindo S, Spruston N, and Cembrowski MS (2020). A sparse, spatially biased subtype of mature granule cell dominates recruitment in hippocampal-associated behaviors. Cell Rep 31, 107551. [PubMed: 32348756]

Fernández-Ruiz A, Oliva A, Soula M, Rocha-Almeida F, Nagy GA, Martin-Vazquez G, and Buzsáki G (2021). Gamma rhythm communication between entorhinal cortex and dentate gyrus neuronal assemblies. Science 372, eabf3119. [PubMed: 33795429]

Fuhrmann F, Justus D, Sosulina L, Kaneko H, Beutel T, Friedrichs D, Schoch S, Schwarz MK, Fuhrmann M, and Remy S (2015). Locomotion, theta oscillations, and the speed-correlated firing of hippocampal neurons are controlled by a medial septal glutamatergic circuit. Neuron 86, 1253–1264. [PubMed: 25982367]

Giovannucci A, Friedrich J, Gunn P, Kalfon J, Brown BL, Koay SA, Taxidis J, Najafi F, Gauthier JL, Zhou P, et al. (2019). CaImAn an open source tool for scalable calcium imaging data analysis. Elife 8, e38173. [PubMed: 30652683]

GoodSmith D, Chen X, Wang C, Kim SH, Song H, Burgalossi A, Christian KM, and Knierim JJ (2017). Spatial representations of granule cells and mossy cells of the dentate gyrus. Neuron 93, 677–690.e5. [PubMed: 28132828]

Grosmark AD, and Buzsáki G (2016). Diversity in neural firing dynamics supports both rigid and learned hippocampal sequences. Science 351, 1440–1443. [PubMed: 27013730]

Grosmark AD, Sparks FT, Davis MJ, and Losonczy A (2021). Reactivation predicts the consolidation of unbiased long-term cognitive maps. Nat. Neurosci 24, 1574–1585. [PubMed: 34663956]

Hainmueller T, and Bartos M (2018). Parallel emergence of stable and dynamic memory engrams in the hippocampus. Nature 558, 292–296. [PubMed: 29875406]

Hargreaves EL, Rao G, Lee I, and Knierim JJ (2005). Major dissociation between medial and lateral entorhinal input to dorsal hippocampus. Science 308, 1792–1794. [PubMed: 15961670]

Hetherington PA, and Shapiro ML (1997). Hippocampal place fields are altered by the removal of single visual cues in a distance-dependent manner. Behav. Neurosci 111, 20–34. [PubMed: 9109621]

Hollup SA, Molden S, Donnett JG, Moser MB, and Moser EI (2001). Accumulation of hippocampal place fields at the goal location in an annular watermaze task. J. Neurosci 21, 1635–1644. [PubMed: 11222654]

Hunsaker MR, Rosenberg JS, and Kesner RP (2008). The role of the dentate gyrus, CA3a,b, and CA3c for detecting spatial and environmental novelty. Hippocampus 18, 1064–1073. [PubMed: 18651615]

Jung D, Kim S, Sariev A, Sharif F, Kim D, and Royer S (2019). Dentate granule and mossy cells exhibit distinct spatiotemporal responses to local change in a one-dimensional landscape of visual-tactile cues. Sci. Rep 9, 9545. [PubMed: 31267019]

Kesner RP (2013). An analysis of the dentate gyrus function. Behav. Brain Res 254, 1–7. [PubMed: 23348108]

Kim S, Kim Y, Lee S-H, and Ho W-K (2018). Dendritic spikes in hippocampal granule cells are necessary for long-term potentiation at the perforant path synapse. Elife 7, e35269. [PubMed: 29578411]

Knierim JJ, and Neunuebel JP (2016). Tracking the flow of hippocampal computation: pattern separation, pattern completion, and attractor dynamics. Neurobiol. Learn. Mem 129, 38–49. [PubMed: 26514299]

Knierim JJ, Neunuebel JP, and Deshmukh SS (2014). Functional correlates of the lateral and medial entorhinal cortex: objects, path integration and local-global reference frames. Philos. Trans. R. Soc. Lond. B, Biol. Sci 369, 20130369. [PubMed: 24366146]

Kohara K, Pignatelli M, Rivest AJ, Jung H-Y, Kitamura T, Suh J, Frank D, Kajikawa K, Mise N, Obata Y, et al. (2014). Cell type-specific genetic and optogenetic tools reveal novel hippocampal CA2 circuits. Nat. Neurosci 17, 269–279. [PubMed: 24336151]

Krueppel R, Remy S, and Beck H (2011). Dendritic integration in hippocampal dentate granule cells. Neuron 71, 512–528. [PubMed: 21835347]

Lee JW, and Jung MW (2017). Separation or binding? Role of the dentate gyrus in hippocampal mnemonic processing. Neurosci. Biobehav. Rev 75, 183–194. [PubMed: 28174077]

Lee JW, Kim WR, Sun W, and Jung MW (2009). Role of dentate gyrus in aligning internal spatial map to external landmark. Learn. Mem 16, 530–536. [PubMed: 19706836]

Leutgeb JK, Leutgeb S, Moser M-B, and Moser EI (2007). Pattern separation in the dentate gyrus and CA3 of the hippocampus. Science 315, 961–966. [PubMed: 17303747]

Luna VM, Anacker C, Burghardt NS, Khandaker H, Andreu V, Millette A, Leary P, Ravenelle R, Jimenez JC, Mastrodonato A, et al. (2019). Adult-born hippocampal neurons bidirectionally modulate entorhinal inputs into the dentate gyrus. Science 364, 578–583. [PubMed: 31073064]

Marr D (1971). Simple memory: a theory for archicortex. Philos. Trans. R. Soc. Lond. B, Biol. Sci 262, 23–81. [PubMed: 4399412]

Maurer AP, and Nadel L (2021). The continuity of context: a role for the Hippocampus. Trends Cogn. Sci 25, 187–199. [PubMed: 33431287]

McHugh TJ, Jones MW, Quinn JJ, Balthasar N, Coppari R, Elmquist JK, Lowell BB, Fanselow MS, Wilson MA, and Tonegawa S (2007). Dentate gyrus NMDA receptors mediate rapid pattern separation in the hippocampal network. Science 317, 94–99. [PubMed: 17556551]

McNaughton BL, Douglas RM, and Goddard GV (1978). Synaptic enhancement in fascia dentata: cooperativity among coactive afferents. Brain Res 157, 277–293. [PubMed: 719524]

O'Keefe J, and Conway DH (1978). Hippocampal place units in the freely moving rat: why they fire where they fire. Exp. Brain Res 31, 573–590. [PubMed: 658182]

O'Keefe J, and Dostrovsky J (1971). The hippocampus as a spatial map. Preliminary evidence from unit activity in the freely-moving rat. Brain Res 34, 171–175. [PubMed: 5124915]

O'Keefe J, and Krupic J (2021). Do hippocampal pyramidal cells respond to nonspatial stimuli? Physiol. Rev 101, 1427–1456. [PubMed: 33591856]

Pnevmatikakis EA, and Giovannucci A (2017). NoRMCorre: an online algorithm for piecewise rigid motion correction of calcium imaging data. J. Neurosci. Methods 291, 83–94. [PubMed: 28782629]

Poucet B, Sargolini F, Song EY, Hangya B, Fox S, and Muller RU (2014). Independence of landmark and self-motion-guided navigation: a different role for grid cells. Philos. Trans. R. Soc. Lond. B Biol. Sci 369, 20130370. [PubMed: 24366147]

Radvansky BA, Oh JY, Climer JR, and Dombeck DA (2021). Behavior determines the hippocampal spatial mapping of a multisensory environment. Cell Rep 36, 109444. [PubMed: 34293330]

Saleem AB, Diamanti EM, Fournier J, Harris KD, and Carandini M (2018). Coherent encoding of subjective spatial position in visual cortex and hippocampus. Nature 562, 124–127. [PubMed: 30202092]

Senzai Y, and Buzsáki G (2017). Physiological properties and behavioral correlates of hippocampal granule cells and mossy cells. Neuron 93, 691–704.e5. [PubMed: 28132824]

Sheffield MEJ, Adoff MD, and Dombeck DA (2017). Increased prevalence of calcium transients across the dendritic arbor during place field formation. Neuron 96, 490–504.e5. [PubMed: 29024668]

Sheintuch L, Rubin A, Brande-Eilat N, Geva N, Sadeh N, Pinchasof O, and Ziv Y (2017). Tracking the same neurons across multiple days in Ca2+ imaging data. Cell Rep 21, 1102–1115. [PubMed: 29069591]

Skaggs WE, McNaughton BL, and Gothard KM (1993). An information-theoretic approach to deciphering the hippocampal code. In Advances in Neural Information Processing Systems 5, Hanson SJ, Cowan JD, and Giles CL, eds. (Morgan-Kaufmann), pp. 1030–1037.

Soltesz I, and Losonczy A (2018). CA1 pyramidal cell diversity enabling parallel information processing in the hippocampus. Nat. Neurosci 21, 484–493. [PubMed: 29593317]

Sun X, Bernstein MJ, Meng M, Rao S, Sørensen AT, Yao L, Zhang X, Anikeeva PO, and Lin Y (2020). Functionally distinct neuronal ensembles within the memory engram. Cell 181, 410–423.e17. [PubMed: 32187527]

Terrazas A, Krause M, Lipa P, Gothard KM, Barnes CA, and McNaughton BL (2005). Self-motion and the hippocampal spatial metric. J. Neurosci 25, 8085–8096. [PubMed: 16135766]

Treves A, and Rolls ET (1994). Computational analysis of the role of the hippocampus in memory. Hippocampus 4, 374–391. [PubMed: 7842058]

Tuncdemir SN, Lacefield CO, and Hen R (2019). Contributions of adult neurogenesis to dentate gyrus network activity and computations. Behav. Brain Res 374, 112112. [PubMed: 31377252]

van Dijk MT, and Fenton AA (2018). On how the dentate gyrus contributes to memory discrimination. Neuron 98, 832–845.e5. [PubMed: 29731252]

Wang C, Chen X, and Knierim JJ (2019). Egocentric and allocentric representations of space in the rodent brain. Curr. Opin. Neurobiol 60, 12–20. [PubMed: 31794917]

Wiener SI, Paul CA, and Eichenbaum H (1989). Spatial and behavioral correlates of hippocampal neuronal activity. J. Neurosci 9, 2737–2763. [PubMed: 2769364]

Witter MP (2007). The perforant path: projections from the entorhinal cortex to the dentate gyrus. Prog. Brain Res 163, 43–61. [PubMed: 17765711]

Woods NI, Stefanini F, Apodaca-Montano DL, Tan IMC, Biane JS, and Kheirbek MA (2020). The dentate gyrus classifies cortical representations of learned stimuli. Neuron 107, 173–184.e6. [PubMed: 32359400]

Zhao X, Wang Y, Spruston N, and Magee JC (2020). Membrane potential dynamics underlying context-dependent sensory responses in the hippocampus. Nat. Neurosci 23, 881–891. [PubMed: 32451487]

Highlights

- Mouse dentate granule cells respond strongly to spatial sensory cues on a treadmill
- Cue cells emerge faster and are more stable than place cells
- Cue cells are weakly modulated by location and place cells by spatially invariant cues
- Cue responses lead to inhibition of other granule cells in the local population

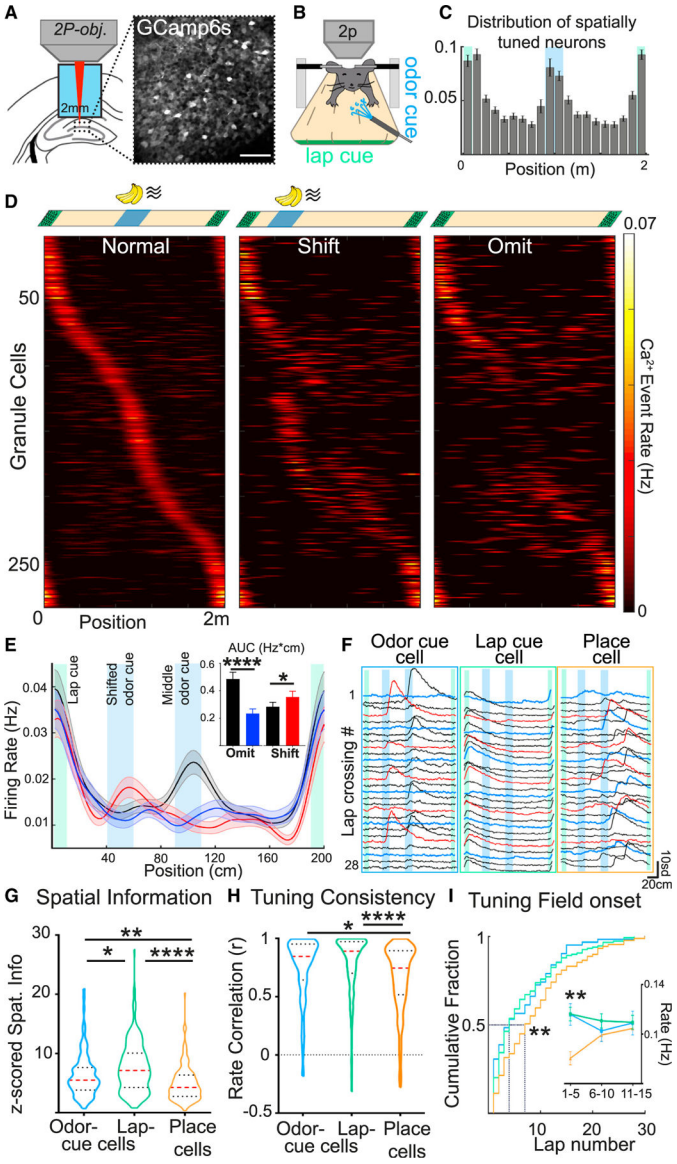

Figure 1. Robust representation of sensory cues in the DG

(A) Two-photon imaging of DG population calcium activity *in vivo* (scale bar, 50 μm).

(B) Behavioral apparatus for sensory cue delivery in the spatial cue task.

(C) Fraction of spatially tuned cells at each treadmill position (n = 4,091 cells, 66 sessions, 8 mice). Locations of the odor and lap cues are shown as blue and green shaded areas, respectively.

(D) Granule cell activity during the spatial cue task. Top: location of the lap cue (green boxes) and an odor cue (blue box) on normal and odor cue shift or omit laps ($n_{\text{normal lap}}$ = 18 ± 4, $n_{\text{shift/omit laps}}$ =6 ± 2). Bottom: lap-averaged spatial firing rates of 285 spatially tuned neurons (N = 8 mice) during the first session with the odor cue on normal middle location (left), cue-shifted (center), and cue-omitted (right) laps. Each row represents activity of a single cell across lap types, sorted by activity on normal middle cue laps.

(E) Average spatial firing rate by position for neurons shown in (D) on normal (black), cue-shifted (red), and cue-omitted laps (blue, mean ± SEM). Inset: averaged area under the firing rate curve within the cue region (AUC; Hz*cm) during normal, cue-shifted, or cue-omitted laps.

(F) Example fluorescence traces from representative odor cue, lap cue, and place cells within a single session. Black, red, and blue traces represent normal, cue-shifted, and omitted laps, respectively.

(G) Spatial information within cue and place cell populations shown in (D).

(H) Tuning consistency of cue and place cells and firing rate correlation between the first and last halves of the session. Red dotted lines in the violin plots show median, and black dotted lines show quartiles.

(I) Emergence of cue and place responses. Cumulative distribution of spatial field onset lap for cue and place cells. Inset: spatial field firing rates of cue and place cells during laps 1–5, 6–10, and 11–15.

Error bars indicate mean ± SEM. See Table S1 for a statistical summary. * < 0.05, **p < 0.01, **** < 0.0001.

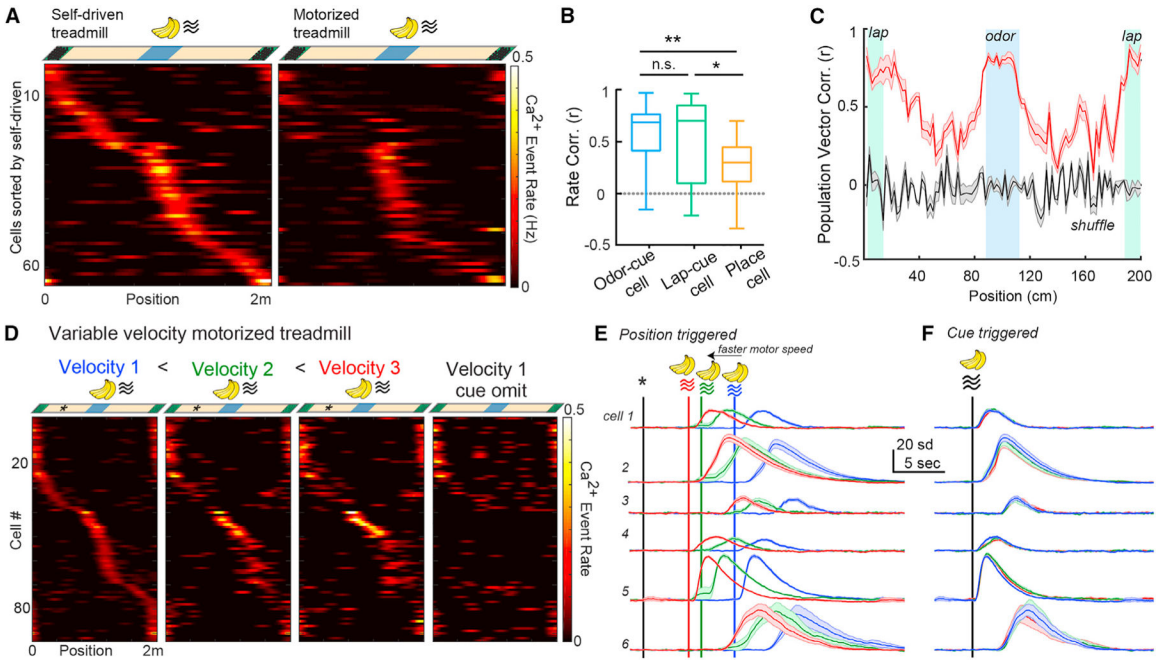

Figure 2. Stable encoding of sensory cues regardless of an animal's locomotive behavior or velocity

(A) Activity of DG granule cells in response to the same odor-cued track during self-driven (left) and motorized (right) treadmill locomotion (n = 67 cells from 5 mice). See also Figures S1C–S1I.

(B)Comparison of average spatial rate correlations in individual neurons tracked across self-driven and motored treadmills shown in (A). Boxes, 25th–75th percentiles; bars, median; whiskers, 99% range. *p < 0.05, **p < 0.01.

(C) PV correlations of spatially tuned neurons between self-driven and motorized treadmills. n = 31 ± 9 cells in 5 mice (red); shaded error bars represent mean ± SEM for each treadmill position. Locations of the middle and lap cue are shown by blue and green shaded areas, respectively. Mean PV correlations by mouse exceeded chance levels, as estimated by shuffling cell identity in each mouse/session (gray).

(D) Granule cell activity during the spatial cue task when the treadmill is motorized at different velocities in each lap, or the cue is omitted randomly (n = 89 spatially tuned neurons from 3 mice). From left to right: velocity 1, 6 cm/s; velocity 2, 9 cm/s; velocity 3, 12 cm/s; cue-omitted laps. Asterisks represent the reference location for position-triggered averages. Each row across all graphs represents a single cell, sorted by each cell's activity on velocity 1 laps. See also Figures S1J and S1K.

(E) Example position-triggered average Ca^{2+} transients from six example cue cells on faster (red), normal (green), and slower (blue) laps.

(F) Example cue-triggered average Ca^{2+} transients from the same cue cells as shown in (E). See Table S1 for a statistical summary.

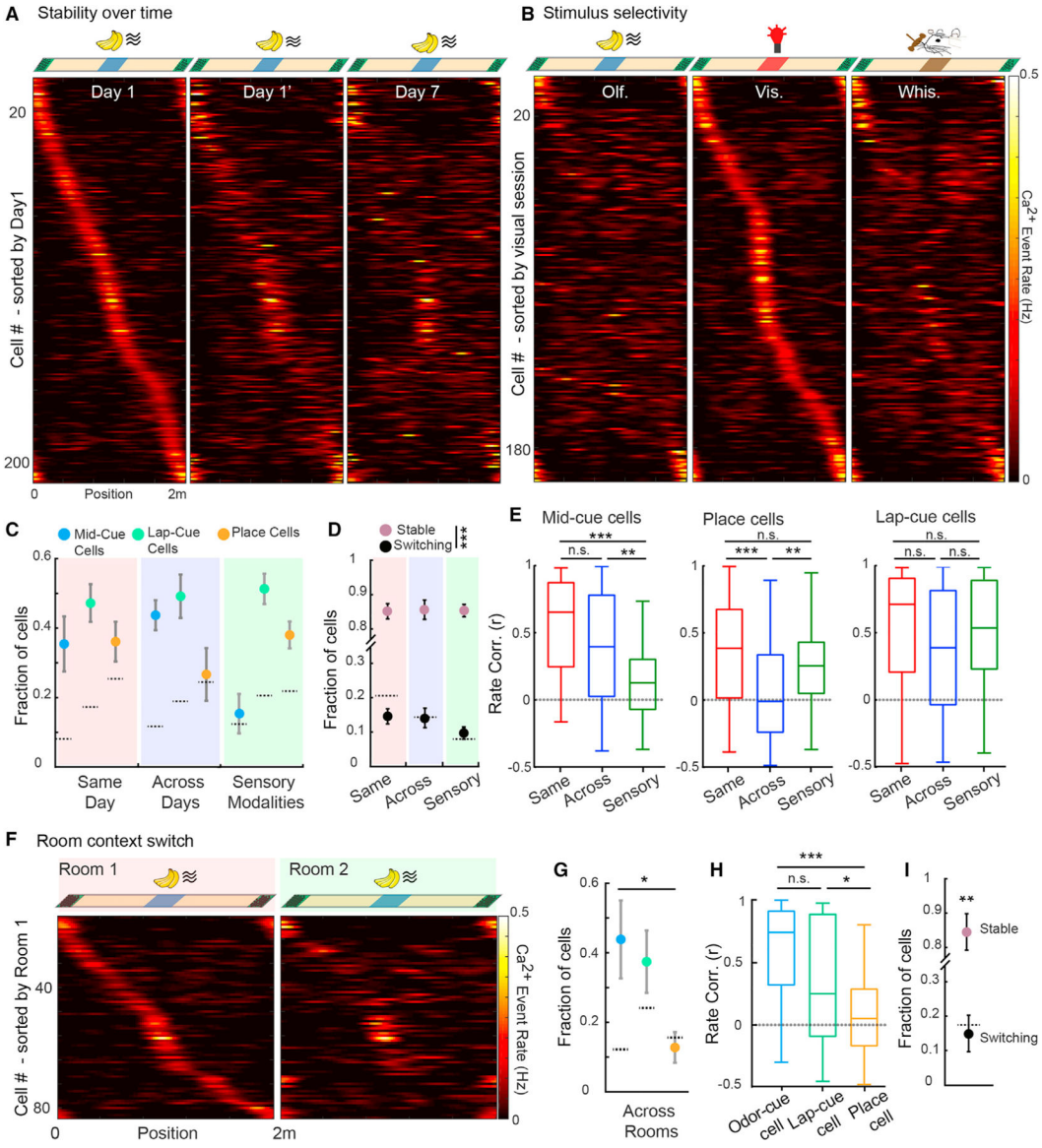

Figure 3. Cue cell responses are stimulus-specific and more stable across days and room contexts than place cells

(A) Spatial firing rates of individual spatially tuned DG granule cells matched between sessions within a day and after 1 week, ordered according to the receptive field location of each cell during the first exposure (n = 233 cells, 8 mice).

(B) Activity of granule cells in response to different sensory cues. Shown are spatial rates for neurons tracked through consecutive sessions during exposure to olfactory, visual, and tactile cues in the middle position. Data are shown for neurons with significant tuning in the visual cue session and tracked in olfactory and whisker tactile cue sessions (n = 196 cells, 6 mice). See also Figures S2A–S2D.

(C) Fraction of cross-session registered cells that encoded the same behavioral variable–lap cue (green), middle cue (blue), or place (orange)–within same day (left), across days (1week, center), and during exposure to different sensory cues (right).

(D) Fractions of spatially tuned cells that stably encoded only one variable (cue or place, pink) or switched response types (cue to place or vice versa, black) within the same day, across days and in response to different sensory cues.
(E) Mean spatial firing rate correlations within the same day (red), over 1 week (“across”, blue), and with different sensory cues (green) for mid-cue cells (left), place cells (center), and lap cue cells (right).
(F) Activity of DG granule cells in response to the same odor-cued track when recorded in different rooms (n = 83 cells, 4 mice). See also Figure S5.
(G) Fraction of individual cells that encoded the same variable–odor cue (blue), lap cue (green), or place (orange)–in different recording rooms.
(H) Comparison of spatial firing rate correlations across cell types in all tuned cells across rooms.
(I) Fractions of spatially tuned cells that stably encode only one variable (cue or place, pink) or switched response types (cue to place or vice versa, black) across different rooms.
Error bars represent mean ± SEM. Dashed lines in panels (C), (D), (G), and (I) represent the 2.5th and 97.5th percentiles of null distributions. See Table S1 for a statistical summary. *$p < 0.05$, **$p < 0.01$, ***$p < 0.001$.

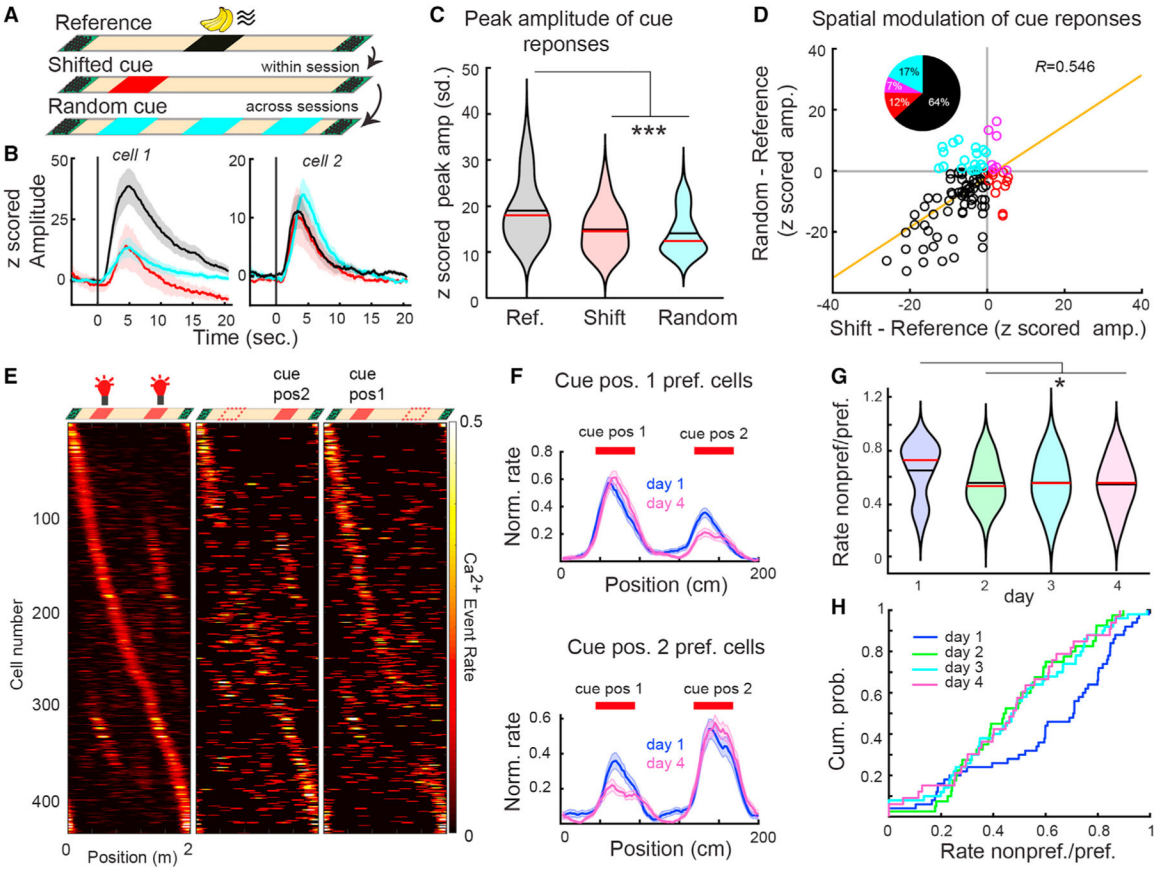

Figure 4. Sensory cue responses are spatially modulated

(A) Effects of cue-location pairing on cue responses. Odor cue response amplitudes are measured for the more frequent middle cue location (black), an intermittently shifted cue location in the same sessions (red), or with random administration of the same cue at one of three positions on each lap in a subsequent session (cyan).

(B) Cue-triggered average Ca^{2+} transients from two example cells.

(C) Peak amplitudes of Ca^{2+} transients from individual odor cue cells under normal, shift, and random cue presentation conditions. Red lines in the violin plots show median, and black lines show mean.

(D) Difference in the magnitude of cue responses in normal laps (“reference”) from random cue and cue shift laps. A yellow line represents linear regression. A pie chart shows the percentage of neurons with higher average responses under normal (black, 64%), cue shift (red, 12%), and random cue presentation conditions (cyan, 17%) and shifted and random laps (purple, 7%).

(E) Dual cue location task. Top: an LED visual cue is given consistently at two positions on the track. Shown is arrangement of cues for normal laps (left, 80% of laps), laps where the first cue is omitted (center, 10%), and laps where the second cue is omitted (right, 10%). Bottom: spatial firing rates of significantly tuned cells on the first day of the task (n = 433 cells, 3 mice).

(F) Average spatial firing rates for cue cells preferring cue position 1 (“pos1”, top) or cue position 2 (“pos2”, bottom) on the first day of the task (blue; n = 25 pos1, n = 25 pos2) and fourth day of the task (pink; n = 13 pos1, n = 20 pos2 cells).
(G) Spatial modulation index (rate for the non-preferred cue/preferred cue location) for all cue cells on days 1–4. Note that lower values mean higher cue spatial selectivity.
(H) Empirical cumulative probability distribution of the spatial modulation index for all cue cells on days 1–4. See also Figures S6A–S6D. Error bars represent mean ± SEM. See Table S1 for a statistical summary. *$p < 0.05$, ***$p < 0.001$.

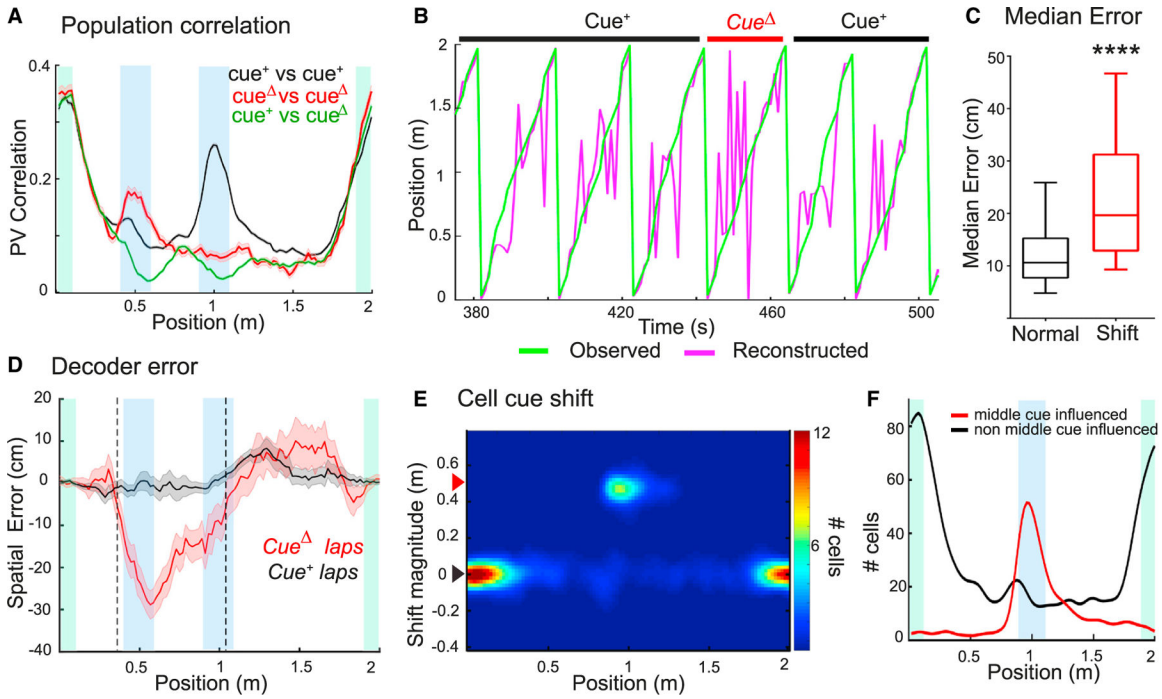

Figure 5. Effects of cue manipulation on spatial encoding

(A) PV correlations for all spatially tuned cells during normal middle cue laps (black), shifted cue laps (red), and pairwise correlations between normal and shifted laps (green).

(B) Example Bayesian decoder prediction of representative normal and cue-shifted laps based on activity from all spatially tuned cells. The green line shows the observed position, and magenta shows the predicted position of the animal.

(C) Average prediction error for normal and cue-shifted laps (n = 66 sessions, 8 mice). Boxes, 25th–75th percentiles; bars, median; whiskers, 99% range.

(D) Spatial decoding error for each treadmill position in normal and cue-shifted laps. Dotted lines indicate the point of statistical equality between normal and cue-shifted lap decoding.

(E) Cell counts for all spatially tuned cells of firing location shift on shifted cue laps (y axis) based on tuning location in normal middle cue laps (x axis), indicating how cells at each position are affected by the cue shift (n = 4,091 cells, 66 sessions, 8 mice). The red arrowhead shows the actual cue shift distance (50 cm), and the black arrowhead indicates no shift relative to middle cue laps.

(F) Mean number of cells not influenced by the odor cue (black; shift magnitude < 0.05 m, “non-middle cue influenced”) and cells shifting precisely along with the cue (red; shift magnitude = 0.5 ± 0.1 m, “middle cue influenced”) at each track position (corresponding to cells in regions of black and red arrowheads in E, respectively).

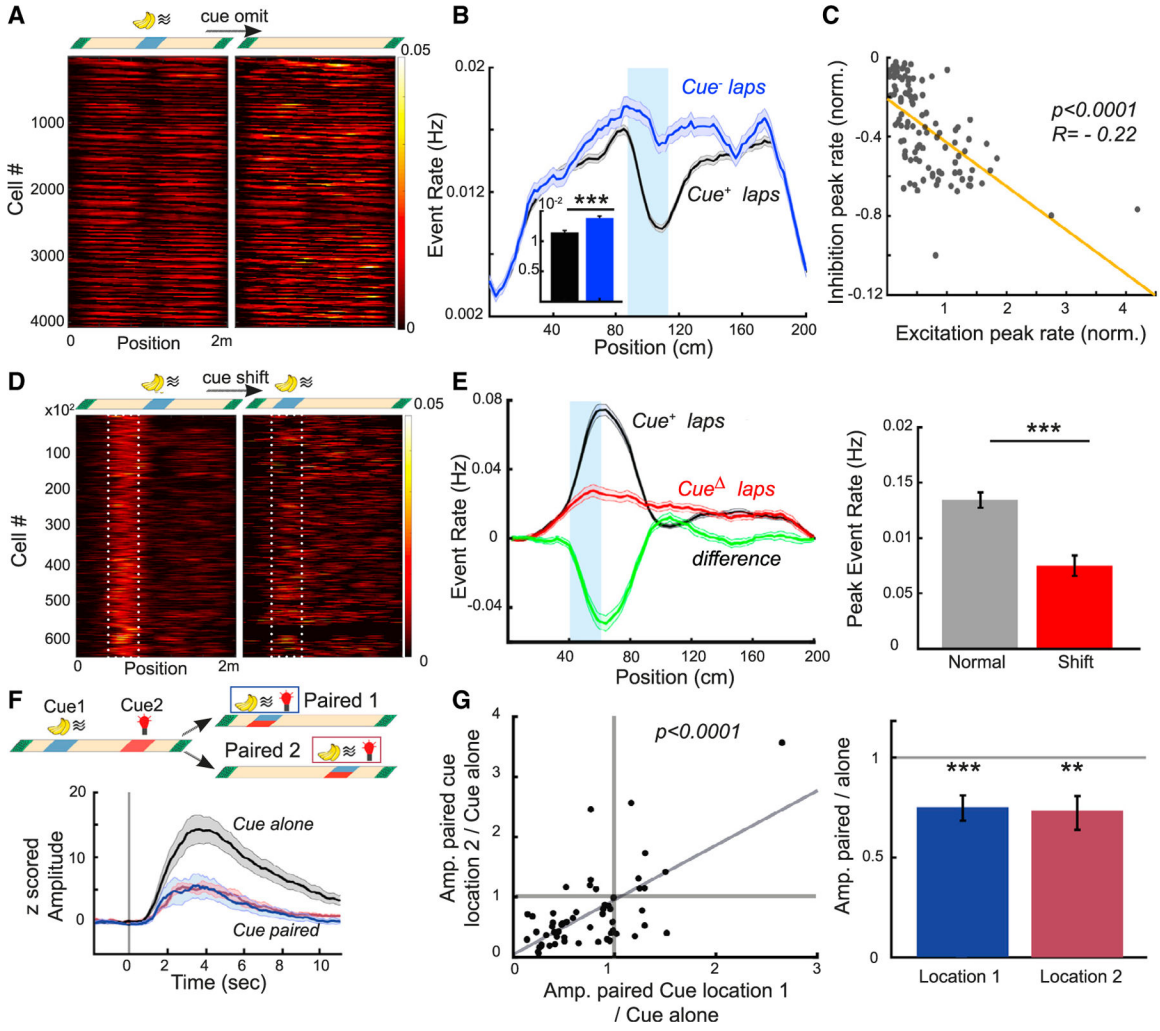

Figure 6. Cue presentation leads to suppression of diverse types of DG responses

(A) Cue-related suppression of spontaneous, out-of-field firing of DG neurons: spatial firing rates outside of the spatial receptive field center of mass (±10 cm) for significantly tuned cells (n = 4,091 cells, 66 sessions, 8 mice) during normal (left) and cue-omitted laps (right).

(B) Average out-of-field firing rates from cells shown in (A) in normal middle cue (black) compared with cue-omitted laps (blue). Inset: average firing rate within the cue delivery position (blue shaded area).

(C) Magnitude of cue-related excitation and inhibition by session: average in-field spatial firing rates (i.e., cue-related excitation) compared with out-of-field, spontaneous firing rates (i.e., cue-related inhibition) at the middle cue location for each session (90–120 cm), adjusted for the pre-cue firing rate. Yellow represents linear regression.

(D) Cue-related suppression of place cell firing: spatial firing rates of place cells (n = 645 cells, 66 sessions, 8 mice) with firing fields at 50–80 cm during normal laps (left) and laps in which the cue is shifted to the same 50-cm location (right).

(E) Left: average spatial firing rate for the above 50- to 80-cm receptive field place cells in normal laps, where the cue is not presented at this location (Cue+, black), compared with

laps in which the cue is shifted to this location (CueD, red; difference in green). Right: average peak firing rate at the shifted cue position of the same place cells as in (D).
(F) Cue-related suppression of cells responding to other distinct cues. Top: diagram of the intermittent cue pairing experiment. Cues of two different modalities were presented at different locations, interspersed with paired presentation at one of these locations on intermittent laps. Bottom: example cue-triggered average Ca^{2+} transients for a cue cell strongly active when the cue is presented alone (black) but with reduced responses when paired with a different cue (blue, pair location 1; purple, location 2).
(G) Left: relative amplitudes of paired cue responses for individual cue cells at the two pairing locations with respect to the response to the cue alone (n = 56 cells, 3 mice). The gray line represents linear fit. Right: average relative response amplitude at the two pairing locations for all cue cells of either type.
Error bars represent mean ± SEM. See Table S1 for a statistical summary. * < 0.05, **p < 0.01, ***p < 0.001.

KEY RESOURCES TABLE

REAGENT or RESOURCE	SOURCE	IDENTIFIER
Antibodies		
Chicken anti-GFP	abcam	Cat#ab13970, RRID:AB_300798
Donkey anti-chicken-AlexaFluor488	Jackson ImmunoResearch	Cat#703-545-155, RRID:AB_2340375
Bacterial and virus strains		
AAV.Syn.GCaMP6s.WPRE.SV40	Addgene	https://www.addgene.org/100843/ Cat#100843-AAV1
pGP-AAV-syn-FLEX-jGCaMP7s-WPRE	Addgene	https://www.addgene.org/104491/ Cat#104491-AAV1
Experimental models: Organisms/strains		
C57BL/6J mice	Jackson Laboratory	Cat#000664; RRID:SCR_004633
Dock-10-Cre mice	Gift from Susumu Tonegawa	Kohara et al. (2014)
Software and algorithms		
MATLAB	Mathworks	RRID:SCR_001622
Suite2p	GitHub	https://github.com/MouseLand/suite2p
NoRMCorre	GitHub	https://github.com/flatironinstitute/NoRMCorre
CellPose	GitHub	https://github.com/MouseLand/cellpose
CellReg	GitHub	https://github.com/zivlab/CellReg
Prism 9	GraphPad	N/A
Original code used in this study	Zenodo	https://doi.org/10.5281/zenodo.5792531